

PAPER • OPEN ACCESS

## Avoidance of axonal stimulation with sinusoidal epiretinal stimulation

To cite this article: Andrea Corna *et al* 2024 *J. Neural Eng.* **21** 026036

View the [article online](#) for updates and enhancements.

### You may also like

- [Selectivity of direct and network-mediated stimulation of the retinal ganglion cells with epi-, sub- and intraretinal electrodes](#)  
David Boinagrov, Susanne Pangratz-Fuehrer, Georges Goetz et al.
- [Model-based analysis of multiple electrode array stimulation for epiretinal visual prostheses](#)  
Jerel K Mueller and Warren M Grill
- [Electronic approaches to restoration of sight](#)  
G A Goetz and D V Palanker



# Breath Biopsy Conference

5th & 6th November  
Online

Join the conference to explore the **latest challenges** and advances in **breath research**, you could even **present your latest work!**

**Register now for free!**

BREATH BIOPSY



- Main talks
- Early career sessions
- Posters



## PAPER

## OPEN ACCESS

RECEIVED  
28 September 2023

REVISED  
12 March 2024

ACCEPTED FOR PUBLICATION  
28 March 2024

PUBLISHED  
10 April 2024

Original content from  
this work may be used  
under the terms of the  
[Creative Commons  
Attribution 4.0 licence](#).

Any further distribution  
of this work must  
maintain attribution to  
the author(s) and the title  
of the work, journal  
citation and DOI.



# Avoidance of axonal stimulation with sinusoidal epiretinal stimulation

Andrea Corna<sup>\*</sup> , Andreea-Elena Cojocaru<sup>ID</sup>, Mai Thu Bui, Paul Werginz<sup>ID</sup> and Günther Zeck<sup>\*</sup>

Institute of Biomedical Electronics, TU Wien, Vienna, Austria

<sup>\*</sup> Authors to whom any correspondence should be addressed.

E-mail: [andrea.corna@tuwien.ac.at](mailto:andrea.corna@tuwien.ac.at) and [guenther.zeck@tuwien.ac.at](mailto:guenther.zeck@tuwien.ac.at)

**Keywords:** electrical stimulation, retina prosthetics, retina implants, CMOS-based microelectrode array, MEA, artificial vision

Supplementary material for this article is available [online](#)

## Abstract

**Objective.** Neuromodulation, particularly electrical stimulation, necessitates high spatial resolution to achieve artificial vision with high acuity. In epiretinal implants, this is hindered by the undesired activation of distal axons. Here, we investigate focal and axonal activation of retinal ganglion cells (RGCs) in epiretinal configuration for different sinusoidal stimulation frequencies. **Approach.** RGC responses to epiretinal sinusoidal stimulation at frequencies between 40 and 100 Hz were tested in *ex-vivo* photoreceptor degenerated (rd10) isolated retinæ. Experiments were conducted using a high-density CMOS-based microelectrode array, which allows to localize RGC cell bodies and axons at high spatial resolution. **Main results.** We report current and charge density thresholds for focal and distal axon activation at stimulation frequencies of 40, 60, 80, and 100 Hz for an electrode size with an effective area of 0.01 mm<sup>2</sup>. Activation of distal axons is avoided up to a stimulation amplitude of 0.23  $\mu$ A (corresponding to 17.3  $\mu$ C cm<sup>-2</sup>) at 40 Hz and up to a stimulation amplitude of 0.28  $\mu$ A (14.8  $\mu$ C cm<sup>-2</sup>) at 60 Hz. The threshold ratio between focal and axonal activation increases from 1.1 for 100 Hz up to 1.6 for 60 Hz, while at 40 Hz stimulation frequency, almost no axonal responses were detected in the tested intensity range. With the use of synaptic blockers, we demonstrate the underlying direct activation mechanism of the ganglion cells. Finally, using high-resolution electrical imaging and label-free electrophysiological axon tracking, we demonstrate the extent of activation in axon bundles. **Significance.** Our results can be exploited to define a spatially selective stimulation strategy avoiding axonal activation in future retinal implants, thereby solving one of the major limitations of artificial vision. The results may be extended to other fields of neuroprosthetics to achieve selective focal electrical stimulation.

## 1. Introduction

Neural interfaces and neuroprosthetics exploit neuromodulation to restore lost motor or sensory functions by stimulating neural networks. Successful neuroprosthetic or neuromodulation applications include stimulation of deep brain nuclei (Limousin *et al* 1998, Deuschl *et al* 2006, Krauss *et al* 2021), of the spinal cord (Lorach *et al* 2023), of the cochlea (Clark 2003, Wilson and Dorman 2008) as well as peripheral nerves (Plachta *et al* 2014). A type of neuroprostheses with mixed outcomes is retinal implants used for the treatment of retinitis pigmentosa or age-related macular degeneration. Although some promising examples of clinical outcomes in implanted

patients have been reported (Humayun *et al* 2012, Muqit *et al* 2019, Cehajic Kapetanovic *et al* 2020), retinal implants have faced setbacks due to unsuccessful designs leading to two companies discontinuing their CE approved devices (Ayton *et al* 2020). New implants are, however, in clinical trials or under testing (Lorach *et al* 2015, Ayton *et al* 2020, Vagni *et al* 2022).

Among the difficulties to restore some visual percepts using retinal prosthetics is the lack of optimal stimulation waveforms. This problem is most obvious in epiretinal configuration, where the unmyelinated axons from peripheral retinal ganglion cells (RGCs) travel towards the optic nerve, thereby crossing the stimulation electrodes. Activation of axons of passage

prevents the possibility to stimulate RGCs with high spatial resolution, thus limiting the visual acuity perceived by the patient. In the absence of selective stimulation, axons of passage are activated, creating misleading elongated percepts in the patients (Nanduri *et al* 2012, Beyeler *et al* 2019). The problem of activation of passing axons may be tackled via closed-loop stimulus optimization algorithms (Grosberg *et al* 2017, Madugula *et al* 2022, Gogliettino *et al* 2023). However, the simplest way to avoid axonal stimulation would be a stimulation waveform capable of activating only the soma or the axon initial segment (AIS) of a target cell, here defined as focal stimulation, without activating nearby distal axons of passage and without requiring prior knowledge of RGC location. In this work, we used sinusoidal waveforms to investigate focal stimulation of RGCs and identified the amplitude and frequency window for such selective activation.

To date, commercial retinal implants apply square pulses in the millisecond range that are likely to activate axons (Ayton *et al* 2020). On the other hand, low-frequency waveforms and especially sinusoidal stimulation, despite showing promising preliminary results, received little attention. In a remarkable study, Weitz *et al* (2015) reported low frequency stimuli to be able to avoid the activation of passing axons and thereby circumvent elongated percepts in one patient. In-vitro experiments corroborated this finding, however, without providing information about the resolution that could be achieved. Single-cell based studies of sinusoidal stimulation had been conducted over the years by the Fried. Through the combination of epiretinal micro-electrode stimulation and simultaneous patch-clamp recordings they identified a window of selective activation up to 25 Hz in the rabbit retina group (Freeman *et al* 2010, Twyford and Fried 2016).

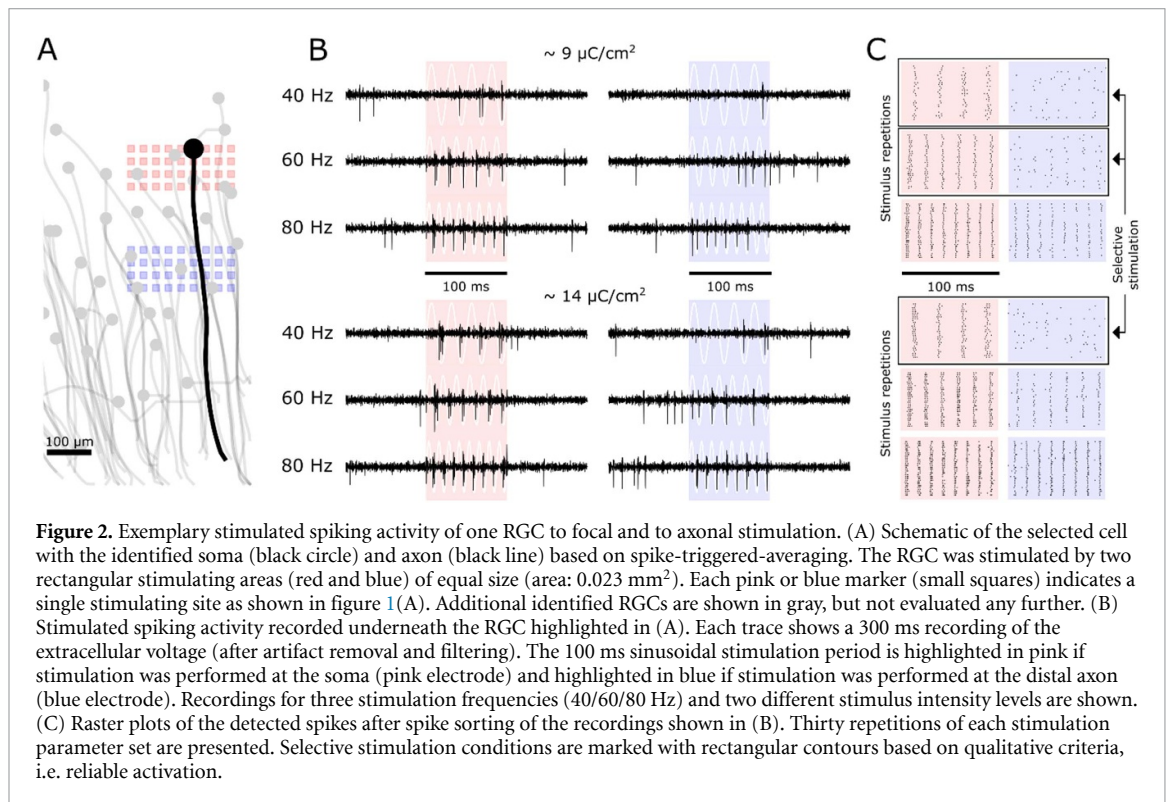
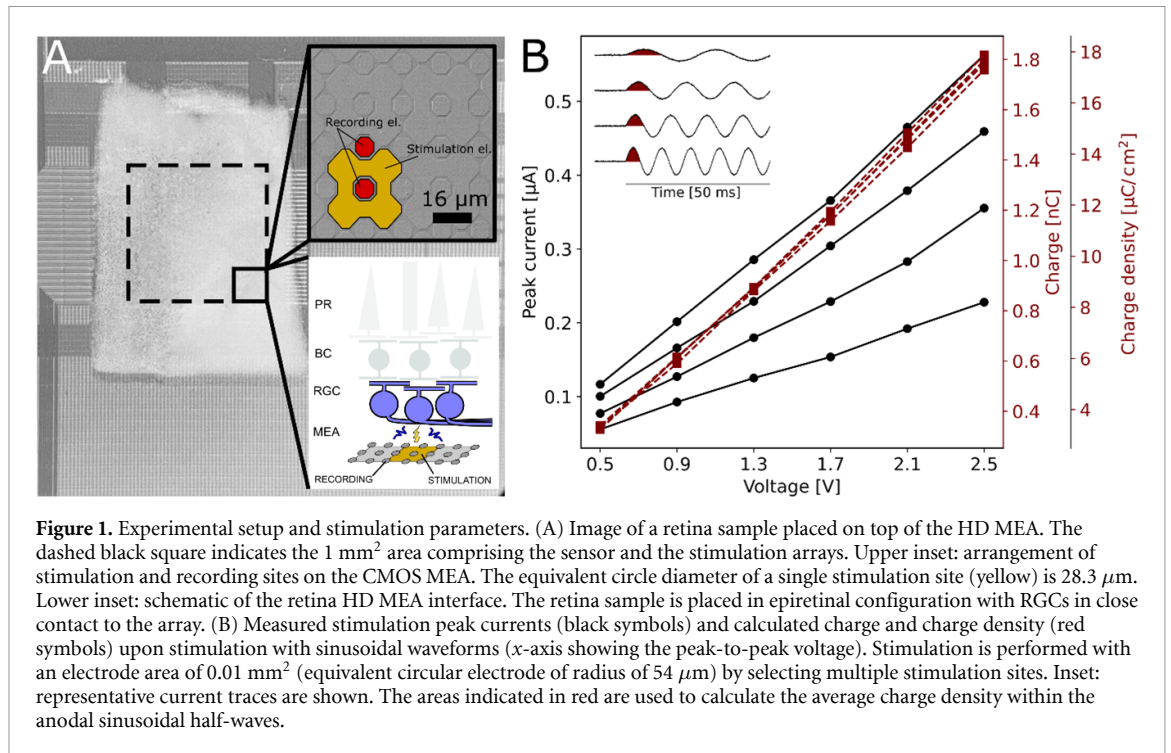
Notably, low-frequency (<200 Hz) sinusoidal waveforms are being utilized in various neuroprostheses, such as spinal cord subperception neuromodulation (Gilbert *et al* 2022), cochlear implants operating with analog waveforms (Stupak *et al* 2018), and specific cases of deep brain stimulation (Xie *et al* 2015). However, none of these applications deals with the delicate and close neighborhood between targeted cell bodies and axons of passage such as in the retina. A first indication for focal epiretinal ganglion cell stimulation in a blind retina was reported recently by our lab (Corna *et al* 2021). There, however, the stimulation was fixed to one frequency (40 Hz) and only a few stimulation amplitudes. Spatially localized stimulation was also reported for epiretinal stimulation using elongated ‘grating-like’ electrodes at the same frequency (40 Hz) and one single amplitude (Cojocaru *et al* 2022). Here, we therefore sought to investigate the effect of sinusoidal

frequencies up to 100 Hz in epiretinal configuration by electrically imaging (Zeck *et al* 2017) RGCs in the *ex-vivo* photoreceptor-degenerated mouse retina. The approach presented here identifies a window of opportunity at frequencies between 40 and 60 Hz, in which focal activation is achieved at lower amplitudes compared to axonal stimulation. As a result, we propose an optimal stimulation strategy that can be implemented to enhance spatial resolution and visual acuity in future retinal implants. The implications of our results extend beyond retinal implants, as they could have valuable applications in various neuroprosthetics scenarios.

## 2. Methods

### 2.1. Extracellular electrophysiology of the *ex vivo* retina

*Ex-vivo* retinæ from rd10 (retinal degeneration 10; B6.CXB1-Pde6brd10/J) and rd10-ChR2 (rd10 expressing ChR2-EYFP, Channelrhodopsin-2—Enhanced Yellow Fluorescent Protein in a subset of RGCs) of age 35–121 d of both genders were used in this study. In addition a single retina sample from a wild type (C57BL/6) expressing ChR2-EYFP was used for the epifluorescence image (figure 5). Dissection of the retina was conducted following previously established protocols (Corna *et al* 2018, 2021). In short, after the removal of the cornea, the lens is extracted exposing the retina. After cutting the eye in two parts the retina is isolated and the vitreous removed. Finally, a portion of the retina (ca. 3–4 mm<sup>2</sup>) is placed on the microelectrode array (MEA) with the RGCs facing downward contacting the sensors (figure 1(A)). Occasionally, gentle pressure with a membrane was applied for a few seconds after the placing to completely flatten the isolated retina on the MEA. Before placing, the MEA was cleaned with 5% Tickopur R36 (Stamm/Berlin), plasma cleaned (Diener electronic) and coated with poly-L-lysine (200 µl, 1 mg ml<sup>-1</sup>, P1399, MW 150–300 kDa, Sigma-Aldrich) to improve adhesion. Retina samples were kept in darkness or dim red light throughout the duration of the recording, and recordings were conducted following 30–45 min of dark adaptation. The explants were continuously perfused with carbogenated Ames medium (A1420, Sigma-Aldrich) at a flow rate of 2–4 ml min<sup>-1</sup> at temperatures ranging from 34 °C to 36 °C. The MEA is connected to the preamplifier mounted on a motorized stage (CONEX CC, Newport) under an upright microscope (BX 50 W, Olympus) with a light source (Cool LED/µMatrix, Rapp OptoElectronic) for light stimulation. The experimental procedures for preparation of the *ex-vivo* retina were approved by the Center for Biomedical Research, Medical University Vienna, Austria.



## 2.2. Complementary metal-oxide-semiconductor based microelectrode arrays (CMOS-MEA)

A CMOS-MEA system (CMOS-MEA5000-System, MultiChannel Systems MCS GmbH) with a total of 4225 recording sites ( $16 \text{ }\mu\text{m}$  pitch) and 1024 stimulation sites ( $32 \text{ }\mu\text{m}$  pitch) covering an area of  $1 \times 1 \text{ mm}^2$  was used (Bertotti *et al* 2014). The area of one single stimulation site is  $632 \text{ }\mu\text{m}^2$  (figure 1(A)), leading to an equivalent circular diameter of  $28.3 \text{ }\mu\text{m}$ .

Recordings were conducted at a sampling rate of 20 kHz except for data from figure 2 which were recorded at a sampling rate of 10 kHz. To eliminate electrical stimulation artifacts, the recorded signals were band-pass filtered in the range of 1–3.5 kHz. In some cases, a wider frequency band was used (figure 2). Spike sorting was performed with the provided software (CMOS-MEA-Tools software, MultiChannel Systems MCS GmbH) based



on an ICA-based algorithm to improve cell detection in the presence of stimulation artifacts (Leibig *et al* 2016). To recover axon positions we performed spike triggered averaging (STA) of the extracellular voltages starting from the spike times output of the spike sorter. The STA algorithm calculates the average voltage signal of a spike across the electrode array by averaging multiple spikes of a single neuron aligned by the spike timing. The result is a voltage trace with reduced noise allowing the detection and tracking of the axonal signal (Zeck *et al* 2011).

### 2.3. Electrical stimulation

Sinusoidal stimulation at frequencies of 40, 60, 80 and 100 Hz were tested. Two different electrode configurations were used in this work: (a) in figure 2(A) two rectangular shaped stimulation electrodes ( $0.023 \text{ mm}^2$ ) were alternatively activated for 100 ms and a break of 100 ms (30 repetitions). The stimulation electrode is a combination of 4 by 9 single stimulation sites. The electrode area was calculated using the effective electrode surface. (b) The data used to calculate the threshold curves (figures 3 and 4) were obtained using a smaller electrode configuration (equivalent area:  $0.01 \text{ mm}^2$ , 4 by 4 single stimulation sites), stimulating for 200 ms with a 200 ms break (50 repetitions).

The stimulation electrodes of the CMOS-MEA work via capacitive stimulation across the dielectric top layer of the chip. The stimulation current density is proportional to the derivative of the applied voltage ( $i_{\text{stim}} = C \times dV/dt$ ). To maximize the capacitance ( $C$ ) the chips used in this study relied on the native oxide of the top titanium nitride electrode without a deposited dielectric layer. The amplitude and waveform of the stimulation current, was measured as voltage drop across a  $10 \text{ } \Omega$  resistor in series to the Ag/AgCl reference electrode (E201ML, Science Products) of the CMOS MEA, using a commercial voltage amplifier (DLPVA, Femto Messtechnik GmbH, Berlin, Germany, (figure 1(B))).

### 2.4. Pharmacological blocking of synaptic transmission

In order to assess the impact of network activity on the evoked responses, we conducted two experiments in which presynaptic inputs to RGCs were blocked pharmacologically (figure 4(D)). In the first experiment we used  $100 \text{ } \mu\text{M}$  DNQX disodium salt (Tocris Cat. no. 2312) in conjunction with the standard Ames medium to inhibit ionotropic glutamatergic synaptic inputs to RGCs. A second, unspecific synaptic blocker ( $100 \text{ } \mu\text{M}$   $\text{CdCl}_2$ ) was applied in a separate series of experiments (Twyford and Fried 2016). Recordings were conducted following a continuous perfusion period of 30 min to ensure thorough drug application. A 1 Hz green full field Flicker stimuli was used to

elicit photoreceptor-mediated visual responses (supplementary figure) to test light responsiveness after the addition of synaptic blockers.

## 3. Data analysis

In order to classify RGCs as focally or axonally activated (figures 3 and 4), we selected a radius of  $96 \text{ } \mu\text{m}$  from the stimulating electrode center. This distance is based on the geometrical dimension of the stimulating electrode, in order to count all cells up to the corner of the electrode. All the RGCs stimuli located inside this radius were marked as focally activated, if they increased the firing rate to stimulation.

Firing rate (FR) was calculated using the average number of spikes during multiple stimulus repetitions (see *electrical stimulation* section for details). The average response is calculated as the average firing rate between all the RGCs considered in the analysis. RGCs were included in the analyzed dataset if their firing rate at the highest stimulation intensity was at least double the firing rate at the lowest stimulation intensity. Additionally, we required the firing rate at the highest intensity to be at least 50% of the stimulation frequency (i.e. on average the RGC should be activated in 50% of the stimulus repetitions). We excluded 3 ms at the beginning and at the end of the stimulus repetition to avoid spikes miscounts due to the stimulation artifact. The normalized firing rate (figure 4) was calculated as  $[\text{FR} - \min(\text{FR})] / [\max(\text{FR}) - \min(\text{FR})]$  and the corresponding error as standard error of the mean divided by the  $\max(\text{FR})$ . Threshold was defined as the amplitude when firing rate reached 50% of the normalized firing rate. Comparisons of means (figure 3) were conducted using a t-test (figure 3).

## 4. Results

### 4.1. Selective activation of RGCs, somatic and axonal responses

The aim of this work is to define a stimulation strategy able to focally activate RGCs while avoiding the stimulation of nearby axons of passage. As a proof of concept of focal activation, we first stimulated a single RGC (figure 2(A)). The cell position was identified by the spike sorting algorithm while the axon trajectory was revealed by spike-triggered-averaging (see methods for details). We selected two rectangular stimulation electrodes each  $0.023 \text{ mm}^2$  in size (from a rectangular combination of 4 by 9 single stimulation sites) separated by  $128 \text{ } \mu\text{m}$  (figure 2(A)). The cell body of the identified RGC was located over one of two electrodes (pink markers) and the axon traversed over the second (blue markers). The stimulation protocol consisted of different intensity levels at three frequencies (40, 60 and 80 Hz). In figure 2(B)

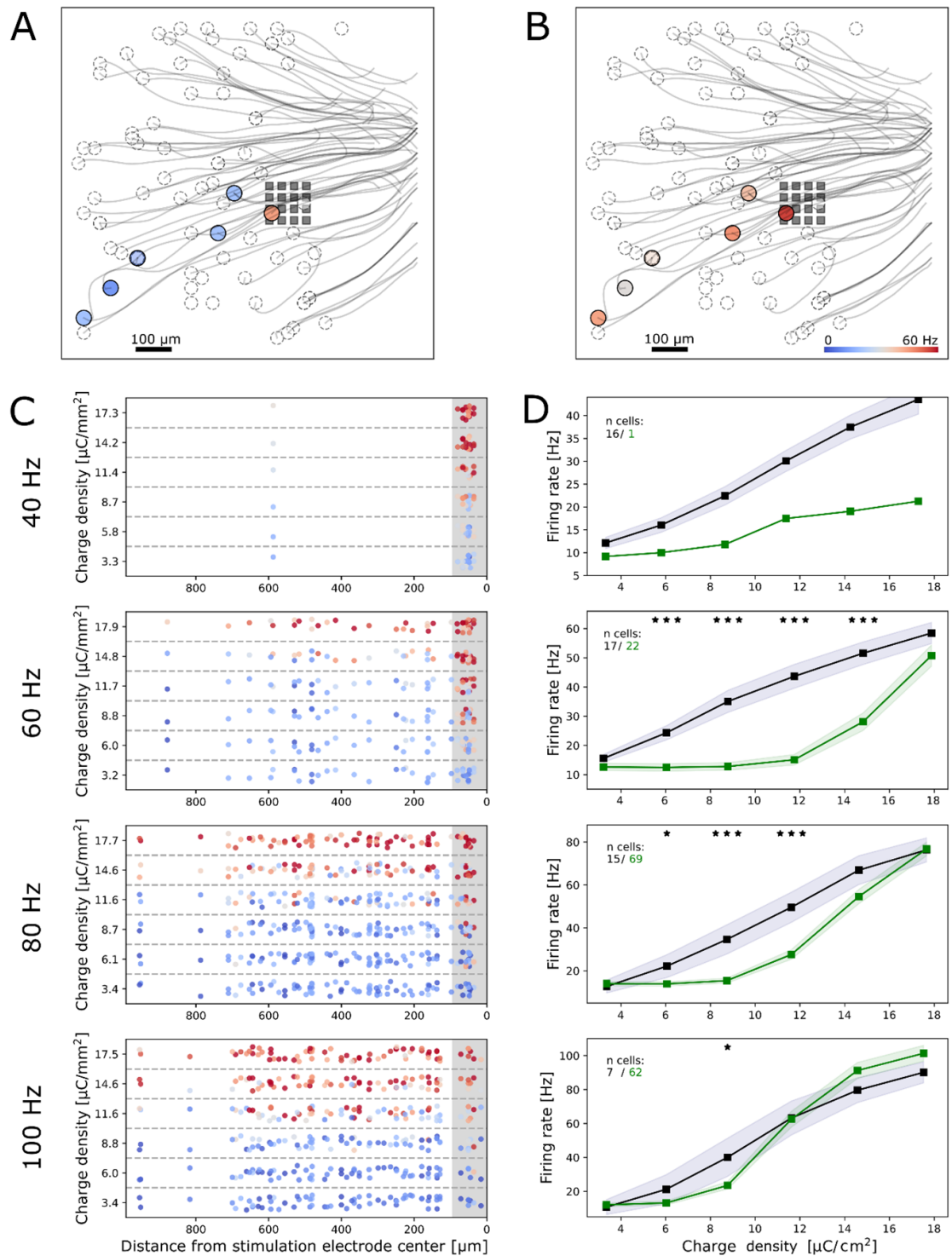
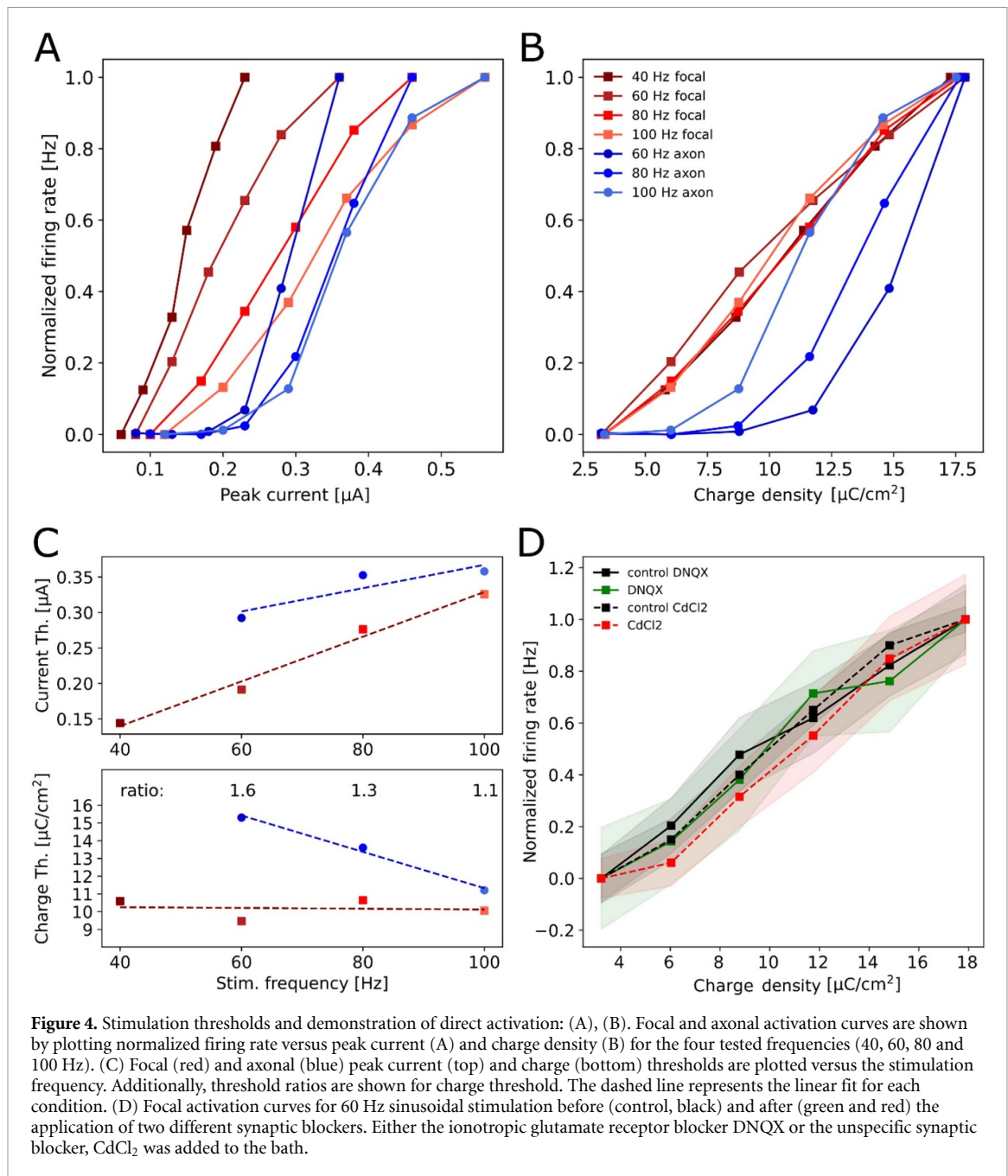


**Figure 3.** Selective activation window: (A)–(B) RGC responses to 60 Hz stimulation with the firing rate color-coded between 0 (blue) and 60 Hz (red) for two different stimulation intensities (A)  $14.8 \mu\text{C cm}^{-2}$ , (B)  $17.9 \mu\text{C cm}^{-2}$ . The colored cells are the ones considered in the analysis, i.e. activated by the stimuli (see methods for details), while all the other RGCs (dashed circles) detected during the recording were not activated. Scale bars in (A)–(B)  $100 \mu\text{m}$ , RGC soma are not to scale. (C) Two dimensional representation of RGCs response versus distance to the stimulation electrode center at different frequencies and charge densities. Each dot represents a single RGC included in the analysis, color coded by the cell firing rate between 0 Hz (blue) and the stimulation frequency (red). Each row along the y-axis comprises all cells stimulated at one stimulus strength and frequency indicated on the y-axis. Rows are separated by a dotted line. Dots representing RGCs are randomly jittered inside a row in the y-direction to avoid overlap. The length of the gray background in the x-direction indicates the RGC distance from the center of the stimulation electrode considered as focal activation (i.e.  $96 \mu\text{m}$ ). (D) Focal (black) and axonal (green) activation curves for the 4 different stimulation frequencies (40, 60, 80 and 100 Hz). For all RGCs the firing rate during stimulation is plotted versus the average stimulation charge measured during one sinusoidal phase. Gray and green shadings indicate the standard error of the mean. The y-axis scaling varies for each stimulation frequency, with the firing rate matching the stimulation frequency at high intensity. Significance levels are indicated as follows: \* =  $p < 0.05$ , \*\* =  $p < 0.01$ , \*\*\* =  $p < 0.001$ .



on the left, the filtered voltage of the recording electrode under the soma during one repetition of 100 ms of continuous stimulation is shown. For the 60 Hz low amplitude stimulation ( $0.4 \mu\text{A}/8.73 \mu\text{C cm}^{-2}$ ), the cell responded reliably if the stimulation electrode was located under the soma (pink). The firing rate increased during the stimulation compared to the spontaneous activity and the cell fired in phase with the cathodic phase of the stimulation current. When instead the electrode under the axon (blue) was activated there was no noticeable response. The same results were obtained for 40 Hz stimulation at high intensity ( $0.43 \mu\text{A}/13.5 \mu\text{C cm}^{-2}$ ). We define this type of stimulation as selective stimulation. In contrast, for stimulation at 80 Hz and at 60 Hz for

higher stimulus intensity ( $0.85 \mu\text{A}/14.1 \mu\text{C cm}^{-2}$  and  $0.64 \mu\text{A}/13.9 \mu\text{C cm}^{-2}$ ), the RGC was activated by stimulation with either one of the two electrodes. If the cell is activated by the distant electrode, an action potential is elicited in the axon, backpropagating to the soma (orthodromic) but also in the direction of the optic nerve (antidromic). Such phenomenon is further referred to as non-selective or axonal activation. All stimulation protocols were presented alternating between the two electrodes for a total of 30 repetitions to qualitatively observe the reliability of activation without fading (figure 2(C)). Although quite illustrative, the stimulation protocol used here employed relatively large electrodes, potentially activating a large part of the presynaptic network and

being spatially unspecific. Therefore, in the following experiments we employ smaller, square-shaped electrodes of  $0.01 \text{ mm}^2$  to obtain a clearer answer regarding spatial selectivity.

#### 4.2. Sinusoidal stimulation allows for selective focal activation of RGCs

Six intensity levels were tested for stimulation with a square shape electrode (area of  $0.01 \text{ mm}^2$ ) and the evoked ganglion cell spiking was evaluated as firing rate (FR) during the stimulation (figures 3(A) and (B)). Cells are marked as focally activated or axonally activated based on the relative position to the stimulation electrode. Cells with the soma located in a radius of  $96 \text{ }\mu\text{m}$  from the electrode center were marked as focally activated. Only activated RGCs, i.e. cells showing an increase in firing rate were considered in the following analysis (see Methods for details). At a stimulation frequency of 40 Hz the firing rate increased linearly up to 40 Hz (i.e. about 1 spike/sinusoidal waveform) for the maximal stimulus intensity of  $0.23 \text{ }\mu\text{A}$  ( $17.3 \text{ }\mu\text{C cm}^{-2}$ ). The positions of all activated RGCs with respect to the electrode center are shown in figure 3(C), with the change in firing rate being color-coded. The qualitative raster plot suggests that the RGC soma or the nearby AIS might be the site of preferred activation. The linear increase in firing rate was observed exclusively for focal activation ( $n = 16$  RGCs), with one exception where the distal axon of one RGC could be stimulated increasing the spontaneous firing rate from  $\sim 10$  to 20 Hz. A similar linear increase of the firing rate was detected for focal activation during 60, 80 and 100 Hz stimulation; the firing rate increased with increasing stimulus strength and reached about 1 spike/sinusoidal waveform at an amplitude of 0.36, 0.46 and  $0.56 \text{ }\mu\text{A}$ , respectively ( $17.9$ ,  $17.7$  and  $17.5 \text{ }\mu\text{C cm}^{-2}$ ). For these stimulation frequencies axonal activation was detected, however with a different property. The axonal activation curves have a steeper increase, i.e. a smaller dynamic range, with the rising onset at higher intensity compared to the focal activation (figure 3(D)). The difference between focal and axonal activation onset decreases with increasing frequency, for example at 60 Hz a large gap is detected between axonal and focal activation curves. This window of opportunity narrows for 80 Hz and closes at 100 Hz, where the two activation curves overlap for most amplitudes. To identify the window of selective activation we performed a *t*-test between the focal and axonal response distribution at each stimulation intensity. The activation curves are an average of multiple cells (40/60/80/100 Hz: focal: 16/17/15/7; axons: 1/22/69/62). For 60, 80 and 100 Hz, we identified a window of selective activation up to 0.28, 0.3 and  $0.29 \text{ }\mu\text{A}$  ( $14.8$ ,  $11.6$  and  $8.8 \text{ }\mu\text{C cm}^{-2}$ ).

#### 4.3. Strength–duration relationship and stimulation mechanism

To better compare the results at different frequencies we investigated the activation curves as normalized firing rate versus the peak stimulation current and versus the charge density calculated within half of the sine wave (figures 4(A) and (B)). Using the normalized firing rate allows to exclude the spontaneous activity from the threshold calculation. Qualitative inspection of the activation curves leads to two results. First, there is a separation between the focal and axonal activation curve, and this difference shrinks when increasing the stimulation frequency. Secondly, the peak current necessary for focal activation of RGCs increased linearly with frequency (red curves in figure 4(A)), which is equivalent to a constant charge needed to achieve a certain activation level, independent of the tested frequency (red curves in figure 4(B)). For axonal activation however this behavior was not observed (blue curves in figure 4(B)).

In order to quantify these two results, we calculated the stimulation threshold as the peak current or charge necessary to reach 50% of the normalized maximal firing rate (see methods for details). Considering that only one cell responded to axonal stimulation for 40 Hz, we excluded it from this part of the analysis. The thresholds for focal activation at 40, 60, 80 and 100 Hz were 0.14, 0.19, 0.28 and  $0.33 \text{ }\mu\text{A}$ , respectively ( $10.6$ ,  $9.5$ ,  $10.6$  and  $10 \text{ }\mu\text{C cm}^{-2}$ ). Thresholds for activation of distal axons at 60, 80 and 100 Hz were 0.29, 0.35 and  $0.36 \text{ }\mu\text{A}$ , respectively ( $15.3$ ,  $13.6$ ,  $11.2 \text{ }\mu\text{C cm}^{-2}$ ). When we analyzed activation threshold versus peak current, both the focal and axonal threshold increased with stimulation frequency (figure 4(C), upper panel). However, the slope for focal threshold increase is steeper with the threshold doubling when doubling the stimulation frequency, similarly to previous results (Freeman *et al* 2010). For the axonal curves instead, the thresholds for 80 and 100 Hz were very similar ( $0.353$  and  $0.358 \text{ }\mu\text{A}$ ). On the other hand, if the normalized firing rate was plotted versus the stimulation charge the focal threshold was constant across frequencies at  $\sim 10 \text{ }\mu\text{C cm}^{-2}$  (figure 4(C), bottom panel) or in other words, the focal activation happened always at the same charge level. The threshold for axonal activation instead linearly decreased from  $\sim 15 \text{ }\mu\text{C cm}^{-2}$  (60 Hz) to  $\sim 10 \text{ }\mu\text{C cm}^{-2}$  (100 Hz). These results suggest that the focal response, potentially via the AIS, and the distal axon response, originates from differences in the strength–duration curve of the two cell elements. This difference results in the window of opportunity for selective stimulation. The relation between focal and axonal threshold at different stimulation frequencies is shown by the change in charge threshold ratios (figure 4(C), bottom panel). The threshold ratio



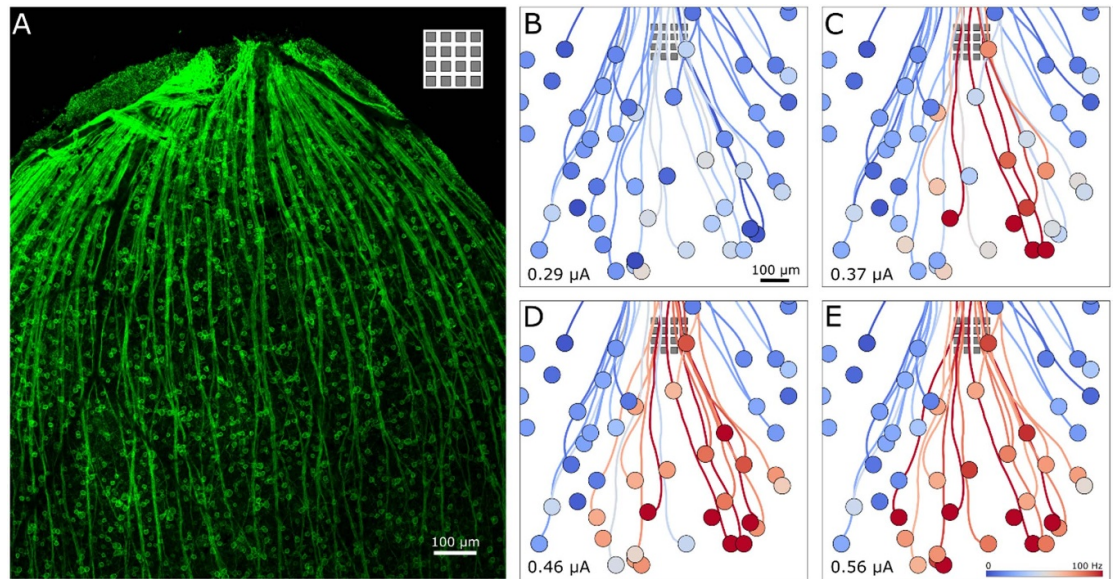


**Figure 5.** Axon bundle stimulation extends the radius of activation: (A) Fluorescence image of somas and axons in a subset of RGCs expressing ChR2-EYFP. The grey + white squares (top right) indicate the size of the stimulation area used to obtain the results shown in figures 3 and 4 and the subplots (B)–(E) of this figure. (B)–(E). Axonal bundle activation. RGC responses to 100 Hz stimulation and four increasing intensity levels. RGC somas (circle size does not correspond to real soma size) and axons are localized via electrical imaging. The firing rate is color-coded from 0 (blue) to 100 Hz (red).

increased from 1.1 to 1.3 and 1.6 reducing the stimulation frequency from 100 to 80 and 60 Hz, respectively. An even higher threshold ratio is expected for 40 Hz, however the maximum stimulation amplitude was limited by the CMOS electronics which allowed us to infer a conservative maximum threshold ratio of 1.64.

The question arises, however, if the hypothesized ‘focal activation’ is actually driven by presynaptic cells, as suggested in the rabbit retina for low-frequency stimulation (Freeman *et al* 2010, Twyford and Fried 2016). Activation of one single spike per sinusoidal waveform, however, suggests direct activation of the RGC without implication of the presynaptic network. To confirm or reject this hypothesis we performed two additional experiments using different synaptic blockers to inhibit the network input to RGCs by either using 100 μM DNQX or 100 μM CdCl<sub>2</sub> (figure 4(D)) (Cohen and Miller 1999, Freeman *et al* 2010). The experiments were conducted in two different retina samples from a young rd10 mouse. At the early stage of degeneration, rd10 mice show photosensitivity that was used to prove the efficacy of the drug by confirming the disappearance of light response after drug application (supplementary figure 1). In figure 4(D) the focal activation curves under control condition, i.e. prior to the drug application, and after drug application are shown. For both blockers there is no significant change among the activation curves indicating that the focal stimulation happens via direct stimulation and not via the network.

#### 4.4. Axon bundles and radius of activation

Despite axonal stimulation being a well-known phenomenon in epiretinal stimulation, the extent of the activation radius and the number of activated RGCs has not been fully clarified. Weitz *et al* (2015) showed thresholds as a function of displacement from electrode center and the extent of the radius of activation via calcium imaging. However, they reported stimulation thresholds one order of magnitude higher compared to the thresholds found in this study, possibly due to the imaging technique. Here we report the radius of activation via electrical imaging with a planar HD MEA that provides a higher sensitivity and temporal resolution up to single spike resolution.

Axons in the retina often form bundles, therefore stimulation electrodes are in the proximity to multiple axons inside a bundle (figure 5(A)). Axonal activation presents a narrow dynamic range, i.e. a steep activation curve (figure 4(A)). This aggravates the problems related to axonal stimulation. As soon as the activation intensity for axons is reached the majority of cells with the axon passing over the stimulation electrode are activated. In figures 5(B)–(E) the firing rate in response to sinusoidal 100 Hz stimulation is shown for 4 different intensity levels (0.29, 0.37, 0.46, 0.56 μA). With an increase of the stimulation intensity from 0.29 to 0.56 μA the majority of the RGCs detected in the 1 mm<sup>2</sup> sensor area with the axon passing over the stimulation electrode are activated and possibly the activation could extend to RGCs located outside the sensor area. The color coded representations in figures 5(B)–(E) underestimate the

real number of activated RGCs as with extracellular electrophysiological recording only a subpopulation of all RGCs in the interface retina is being recorded. Interestingly, due to axon trajectories in the retina the distance of the RGC to the stimulation electrode does not affect the response (figures 3(C) and 5(C)–(E)).

## 5. Discussion

Here, we report on the selectivity window of electrical stimulation using low-frequency sinusoidal (40–100 Hz) waveforms as a technique to improve the outcome in retinal implants. Our experiments demonstrate that sinusoidal stimulation, within the range of 40–60 Hz selectively activates RGCs while avoiding the distal axons of passage. All results were obtained in epiretinal configuration in photoreceptor degenerated *ex-vivo* retinas (rd10) to mimic implantation conditions *in vitro*. Our findings support the possibility of sinusoidal stimulation as a promising approach for future retinal implants.

### 5.1. Spatially selective activation of RGCs in epiretinal configuration

In this work we demonstrate that sinusoidal waveforms can selectively target the soma or AIS of RGCs (focal activation) while avoiding the activation of distal axons passing over the stimulation electrode. Our findings demonstrate, for the first time, a significant difference in the activation threshold between soma/AIS and distal axon at frequencies of 40 and 60 Hz. Focal selective stimulation at lower frequencies, up to 25 Hz, was previously shown by Weitz *et al* (2015) who demonstrated that axonal stimulation can be reduced by 16 ms square pulses or completely avoided by 25 ms square pulses or 25 Hz sinusoidal stimulation. Freeman *et al* (2010) also reported similar findings with 10 and 25 Hz sinusoidal waveforms for RGCs recorded by the patch-clamp technique. They also presented a similar relation as shown in this work between stimulation threshold and stimulation frequency; however at higher stimulation currents and partially involving the retinal network.

Compared to other approaches such as square pulse stimulation sinusoidal stimulation displays a higher degree of selectivity. It has been shown that optimization of the square pulse parameters, i.e. duration and asymmetry, or the stimulus orientation can increase square pulse selectivity (Esler *et al* 2018, Chang *et al* 2019, Paknahad *et al* 2020). However, the stimulus current used in those studies was orders of magnitude higher to the results presented here. A possible explanation could be the recording technique, with calcium imaging requiring the generation of multiple spikes for reaching detection threshold. Other studies, using MEA recordings, with stimulation currents in the range of the one applied here do not show any difference between axonal and focal

threshold, or even a bias towards axonal stimulation (Madugula *et al* 2022, Gogliettino *et al* 2023). In case of non-selective stimulation, focal activation could be achieved with the use of small electrodes on bidirectional implants (Shah and Chichilnisky 2020). By recording spontaneous RGCs activity it is possible to infer the stimulus sensitivity of specific RGCs and use the information to target single cells via the soma or the axon (Madugula *et al* 2022, Gogliettino *et al* 2023). However, questions arise regarding the percentage of cells that can be a single target over the total population with this approach.

It must be considered that all state-of-the-art MEAs, like the one used here, only allow for the recording of a subset of the total RGC population. The generalization of the results from the cells presented in figure 3 to a broader statement about axonal avoidance may be clarified in future work involving alternative recording methods.

### 5.2. Considerations regarding sinusoidal stimulation in epiretinal implants

Before discussing the feasibility of sinusoidal stimulation in an epiretinal implant we would like to clarify that the CMOS-based capacitive device presented here served only as a bidirectional tool for experimental purposes. We do not expect such device to be implanted for several reasons, including stiffness of the CMOS chip, low stimulation charge achievable by the capacitive electrodes and power requirements.

Given the challenge of powering a portable device implanted inside a moving organ like the eye, retinal implants require low power consumption. This becomes even more critical given the recent transition of the device from wired to wireless photovoltaic control (Boinagrov *et al* 2013, Corna *et al* 2018, Ayton *et al* 2020). In the context of stimulation from the epiretinal side, we were able to achieve focal activation with a peak current of 0.23  $\mu\text{A}$  for 40 Hz (corresponding to a charge density of 10.6  $\mu\text{C cm}^{-2}$ ) and 0.36  $\mu\text{A}$  (9.5  $\mu\text{C cm}^{-2}$ ) for 60 Hz, respectively. These values are slightly smaller compared to the reported values for epiretinal square pulses ( $\sim 1 \mu\text{A}$ ) (Madugula *et al* 2022, Gogliettino *et al* 2023). A bias towards lower thresholds for sinusoidal stimulation has been also reported by other studies, using calcium imaging, when comparing 20 Hz pulses to 20 Hz sinusoidal pulses (Weitz *et al* 2015). Our results also show that focal activation occurs within the first cycle of the sinusoidal stimulus (figure 2(B)), without the need for continuous stimulation. An important consideration beyond the results presented here, relates to the feasibility of sinusoidal stimulation in a retinal implant. Recent work suggests implementation of the sinusoidal signal generator either at a remote location from the stimulation electrode itself (Schütz *et al* 2020) or as a system-on-chip (Löhler *et al* 2023) at the cost of spatial resolution.

When comparing *in vitro* thresholds to clinical data from patients with an epiretinal implant (Chris *et al* 2006, de Balthasar *et al* 2008) we note a difference by about two orders of magnitude. In clinical settings the threshold charge density for short pulses ( $\sim 1$  ms) ranged between  $\sim 50$  up to  $500 \mu\text{C cm}^{-2}$ . The increased thresholds are mainly caused by a relatively large distance between the stimulating electrode and the retina. A tight contact *in vivo* may be achieved by conformal (Lohmann *et al* 2019, Zhou *et al* 2023), flexible (Ferlauto *et al* 2018) or 3D (Steins *et al* 2022) electrode arrays. If tight interfacing fails, the change of preferential activation with vertical displacement needs to be considered. Modeling work (Schiefer and Grill 2006, Mueller and Grill 2013) demonstrated that for short pulses preferential, focal activation of RGCs does not deteriorate for short anodic or cathodic current pulses up to vertical displacements of  $150 \mu\text{m}$ . A conceptually similar modeling is required for sinusoidal stimuli, guided by our experimental results and those of others (Freeman *et al* 2010, Twyford and Fried 2016). Modeling should also consider RGC density and the stacked RGC layers in the human retina close to the fovea.

Avoidance of axonal stimulation aims to improve spatial resolution. However, the spatial resolution achievable with sinusoidal waveforms needs to be tested, since RGCs surrounding the stimulation electrode may be activated. Previous work using small object stimulation demonstrated discrimination of  $32 \mu\text{m}$  spatial jitter for 40 Hz stimulation, which translates to  $1^\circ$  of visual angle (Corna *et al* 2021). In the same work a radius of activation proportional to the electrode size was reported, potentially superior to the one shown for 25 ms pulses (Weitz *et al* 2015). Similar results were found using grating stimulation, closely matching the spatial resolution achieved by optogenetic stimulation (Cojocaru *et al* 2022). These *in vitro* findings need to be validated in clinical settings. A challenge may constitute the spread of the electric field above the stimulation electrodes, which ideally should penetrate the retina perpendicular to the electrode surface (Spencer *et al* 2016).

Lastly, a strategy for encoding visual stimuli needs to be developed. One key consideration is whether low frequency sine waves can provide the necessary stimulation frequency for rate coding. Weitz *et al* demonstrated that 25 Hz pseudo-sinusoidal stimulation was able to evoke percept in patients, suggesting promising results for this approach (2015). Here we demonstrate that even higher stimulation frequency, in the range of human flicker fusion and potentially providing continuous percepts to patients (Mankowska *et al* 2021), can retain selectivity. Nonetheless, several open questions remain regarding the required spike rate and frequency for effective visual information encoding. A second important aspect is contrast encoding. Previous work suggested

encoding contrast by changing the stimulation frequency but not the stimulation amplitude (Nanduri *et al* 2012). Indeed, such strategy would circumvent increased percepts by a radially spreading increasing electric field. However, our results (figure 4) indicate that with such strategy the spatial selectivity is lost above 60 Hz and therefore only a restricted contrast range may be achievable. We have shown previously under laboratory conditions that contrast encoding with sinusoidal stimulation can be achieved (Corna *et al* 2021); however, under ideal experimental conditions involving a reference electrode in the subretinal space.

### 5.3. The mechanism underlying focal activation with sinusoidal stimulation

To fully understand the mechanism of RGC activation during sinusoidal stimulation, we investigated the activation curves versus the applied peak current and the charge within one half sinusoidal phase. RGCs respond in the cathodic phase of the sinus in line with previous reports in epiretinal configuration (Eickenscheidt *et al* 2012, Boinagrov *et al* 2014, Twyford and Fried 2016). Previous studies indicated that low frequency stimulation in the healthy retina operates via network-mediated activation (Freeman *et al* 2010, Twyford and Fried 2016). Our results, in photoreceptor-degenerated retinas, show that sinusoidal stimulation, for the frequencies tested, acts via direct stimulation. Once the network component is ruled out, focal activation may occur via the stimulation of the AIS, of the soma or of the dendritic tree. We therefore use the general term ‘focal activation’ in this work. The AIS represents the section of RGCs with the highest sodium channel density and therefore the lowest local stimulation threshold (Fried *et al* 2009, Werginz *et al* 2020, Kish *et al* 2023, Radivojevic *et al* 2016). Therefore, the most natural conclusion is that the focal activation reported here happens with the AIS in close proximity to the stimulation electrodes and the two different cellular compartments AIS and distal axon, have different strength-duration relationships. Indeed, compartmental modeling for short ( $< 1$  ms) square pulses and the concept of the activating function (Rattay *et al* 2012) may explain the constant charge threshold (figure 4(C)) we report here for focal activation. Future modeling work and a wider stimulation range are needed to clarify if threshold charge density remains constant for sinusoidal stimulation at low frequencies.

Interestingly, sinusoidal selective stimulation has been reported both here with the use of planar MEA, where a high resistivity cleft is formed between the electrodes and the RGCs (Zeitler *et al* 2011) and with single stimulating electrodes  $\sim 20 \mu\text{m}$  above the RGC layer (Freeman *et al* 2010). The tight interface between RGCs and the electrodes in our configuration partially explains the low threshold values. A



second contribution likely comes from the so-called activating function (Rattay 1988) at the electrode edge of extended electrodes (Eickenscheidt and Zeck 2014, Paknahad *et al* 2020).

A final consideration needs to be done regarding cell type specificity. The retina does not operate as a simple light detector but occupies a crucial role in the first steps of visual processing. RGCs are classified in cell types based on many different parameters, such as their receptive field or morphology (Baden *et al* 2016, Goetz *et al* 2022). Despite several different and complex cell types have been already identified, in the field of retinal implants, generally a simplified separation in two major RGC classes, ON and OFF, cells is used. Achieving cell type specificity will represent a turning point, significantly improving the performance of artificial vision. Unfortunately, cell type specific stimulation still remains elusive. The stimulation reported here due to a direct mechanism should target equally ON and OFF RGCs. Some work has been done to identify cell-specific stimuli (Freeman *et al* 2010, Twyford and Fried 2016, Oesterle *et al* 2020) but a definitive conclusion is missing.

#### 5.4. Importance for future retinal implants

Up to date, artificial vision approaches due to the constraint of electrical neuromodulation have been limited as a tradeoff between spatial and temporal resolution and visual field size. Currently, subretinal implants offer superior spatial resolution and subsequent visual acuity and reported the best clinical results (Cehajic Kapetanovic *et al* 2020). However, their visual field is restricted due to the requirement of subretinal implantation (Lorach *et al* 2015). On the other hand, there is a growing emphasis on the significance of a large visual field, which can only be achieved in epiretinal configuration (Ghezzi 2023). Nevertheless, epiretinal implants so far faced challenges in spatial resolution especially due to axonal stimulation. In this work we demonstrated that sinusoidal stimulation can provide a potential solution to the problem via spatially selective activation.

## 6. Conclusion

Here, we present our findings investigating the efficacy of sinusoidal stimulation of the *ex vivo* retina. Experiments were conducted in epiretinal configuration using a HD MEA that provided a high resolution bidirectional interface with photoreceptor degeneration mouse models (rd10) explanted retina. Through our experiments, we have demonstrated, for the first time, that sinusoidal stimulation, within the range of 40–60 Hz, exhibits selective focal stimulation at low charge density via direct activation. Collectively, these findings provide strong support for the efficacy

of sinusoidal stimulation in epiretinal stimulation, potentially leading to advancements in future visual prosthetics.

## Data availability statement

The data cannot be made publicly available upon publication because they are not available in a format that is sufficiently accessible or reusable by other researchers. The data that support the findings of this study are available upon reasonable request from the authors.

## Acknowledgments

This work was supported by the Hochschuljubiläumsfonds der Stadt Wien (H-864102/2022), The European Union's Horizon 2020 research and innovation programme Entrain Vision under the Marie Skłodowska-Curie Grant Agreement No. 861423 and the Austrian Science Fund (FWF) (10.55776/P35488). For open access purposes, the author has applied a CC BY public copyright license to any author accepted manuscript version arising from this submission. The authors thank Viktória Király for the fluorescence image included in the work.

## Author contributions

A C analyzed the data, performed parts of the experiments, and wrote the manuscript. A-E C contributed to data collection in a subset of experiments and participated in the data analysis process. G Z contributed to the experimental design and manuscript writing. P W provided valuable input during manuscript preparation and participated in the discussions. M T B assisted with the execution of experimental procedures. All authors contributed to the article and approved the submitted version.

## Conflict of interest

The authors declare that the research was conducted in the absence of any commercial or financial relationships that could be construed as a potential conflict of interest.

## ORCID iDs

Andrea Corna  <https://orcid.org/0000-0002-3209-6719>

Andreea-Elena Cojocaru  <https://orcid.org/0000-0002-0830-1727>

Paul Werginz  <https://orcid.org/0000-0002-3441-3167>

Günther Zeck  <https://orcid.org/0000-0003-3998-9883>



## References

- Ayton L N *et al* 2020 An update on retinal prostheses *Clin. Neurophysiol.* **131** 1383–98
- Baden T, Berens P, Franke K, Román Rosón M, Bethge M and Euler T 2016 The functional diversity of retinal ganglion cells in the mouse *Nature* **529** 345–50
- Balthasar C D, Patel S, Roy A, Freda R, Greenwald S, Horsager A, Mahadevappa M, Yanai D, McMahon M J and Humayun M S 2008 Factors affecting perceptual thresholds in epiretinal prostheses *Invest. Ophthalmol. Vis. Sci.* **49** 2303–14
- Bertotti G, Velychko D, Dodel N, Keil S, Wolansky D, Tillak B, Schreier M, Grall A, Jesinger P and Röhler S 2014 A CMOS-based sensor array for in-vitro neural tissue interfacing with 4225 recording sites and 1024 stimulation sites 2014 *IEEE Biomedical Circuits and Systems Conf. (BioCAS) Proc.* (IEEE) pp 304–7
- Beyeler M, Nanduri D, Weiland J D, Rokem A, Boynton G M and Fine I 2019 A model of ganglion axon pathways accounts for percepts elicited by retinal implants *Sci. Rep.* **9** 9199
- Boinagrov D, Pangratz-Fuehrer S, Goetz G and Palanker D 2014 Selectivity of direct and network-mediated stimulation of the retinal ganglion cells with epi-, sub- and intraretinal electrodes *J. Neural Eng.* **11** 026008
- Boinagrov D, Pangratz-Fuehrer S, Mathieson K, Goetz G, Galambos L and Palanker D 2013 Intra-retinal electrical stimulation: comparison to epi- and sub-retinal approaches *Invest. Ophthalmol. Vis. Sci.* **54** 1025–25
- Cehajic Kapetanovic J, Troelsenberg N, Edwards T L, Xue K, Ramsden J D, Stett A, Zrenner E and MacLaren R E 2020 Highest reported visual acuity after electronic retinal implantation *Acta Ophthalmol.* **98** 736–40
- Chang Y C, Haji Ghaffari D, Chow R H and Weiland J D 2019 Stimulation strategies for selective activation of retinal ganglion cell soma and threshold reduction *J. Neural Eng.* **16** 026017
- Chris S, Hottowy P, Sher A, Wladyslaw Dabrowski A M L and Chichilnisky E J 2006 Electrical stimulation of mammalian retinal ganglion cells with multielectrode arrays *J. Neurophysiol.* **95** 3311–27
- Clark G 2003 *Cochlear Implants: Fundamentals and Applications* (Springer)
- Cohen E D and Miller R F 1999 The network-selective actions of quinoxalines on the neurocircuitry operations of the rabbit retina *Brain Res.* **831** 206–28
- Cojocaru A E, Corna A, Reh M and Zeck G 2022 High spatial resolution artificial vision inferred from the spiking output of retinal ganglion cells stimulated by optogenetic and electrical means *Front. Cell Neurosci.* **16** 1033738
- Corna A, Herrmann T and Zeck G 2018 Electrode-size dependent thresholds in subretinal neuroprosthetic stimulation *J. Neural Eng.* **15** 045003
- Corna A, Ramesh P, Jetter F, Lee M J, Macke J H and Zeck G 2021 Discrimination of simple objects decoded from the output of retinal ganglion cells upon sinusoidal electrical stimulation *J. Neural Eng.* **18** 046086
- Deuschl G, Schade-Brittinger C, Krack P, Volkmann J, Schäfer H, Bötzel K, Daniels C, Deutschländer A, Dillmann U and Eisner W 2006 A randomized trial of deep-brain stimulation for Parkinson's disease *New Engl. J. Med.* **355** 896–908
- Eickenscheidt M, Jenkner M, Thewes R, Fromherz P and Zeck G 2012 Electrical stimulation of retinal neurons in epiretinal and subretinal configuration using a multicapacitor array *J. Neurophysiol.* **107** 2742–55
- Eickenscheidt M and Zeck G 2014 Action potentials in retinal ganglion cells are initiated at the site of maximal curvature of the extracellular potential *J. Neural Eng.* **11** 036006
- Esler T B, Kerr R R, Tahayori B, Grayden D B, Meffin H and Burkitt A N 2018 Minimizing activation of overlying axons with epiretinal stimulation: the role of fiber orientation and electrode configuration *PLoS One* **13** e0193598
- Ferlauto L, Airaghi Leccardi M J, Chenais N A, Gilliéron S C, Vagni P, Bevilacqua M, Wolfensberger T J, Sivula K and Ghezzi D 2018 Design and validation of a foldable and photovoltaic wide-field epiretinal prosthesis *Nat. Commun.* **9** 992
- Freeman D K, Eddington D K, Rizzo J F 3rd and Fried S I 2010 Selective activation of neuronal targets with sinusoidal electric stimulation *J. Neurophysiol.* **104** 2778–91
- Fried S I, Aaron C W L, Neal J D, Donald K E and Rizzo J F 3rd 2009 Axonal sodium-channel bands shape the response to electric stimulation in retinal ganglion cells *J. Neurophysiol.* **101** 1972–87
- Ghezzi D 2023 The role of the visual field size in artificial vision *J. Neural Eng.* **20** 023001
- Gilbert J E, Titus N, Zhang T, Esteller R and Grill W M 2022 Surround inhibition mediates pain relief by low amplitude spinal cord stimulation: modeling and measurement *eNeuro* **9** ENEURO.0058–22.2022
- Goetz J, Jessen Z F, Jacobi A, Mani A, Cooler S, Greer D, Kadri S, Segal J, Shekhar K and Sanes J R 2022 Unified classification of mouse retinal ganglion cells using function, morphology, and gene expression *Cell Rep.* **40** 111040
- Gogliettino A R *et al* 2023 High-fidelity reproduction of visual signals by electrical stimulation in the central primate retina *J. Neurosci.* **43** 4625–41
- Grosberg L E *et al* 2017 Activation of ganglion cells and axon bundles using epiretinal electrical stimulation *J. Neurophysiol.* **118** 1457–71
- Humayun M S *et al* Argus II Study Grp 2012 Interim results from the international trial of second sight's visual prosthesis *Ophthalmology* **119** 779–88
- Kish K E, Lempka S F and Weiland J D 2023 Modeling extracellular stimulation of retinal ganglion cells: theoretical and practical aspects *J. Neural Eng.* **20** 026011
- Krauss J K *et al* 2021 Technology of deep brain stimulation: current status and future directions *Nat. Rev. Neurol.* **17** 75–87
- Leibig C, Wachtler T and Zeck G 2016 Unsupervised neural spike sorting for high-density microelectrode arrays with convolutive independent component analysis *J. Neurosci. Methods* **271** 1–13
- Limousin P, Krack P, Pollak P, Benazzouz A, Ardouin C, Hoffmann D and Benabid A-L 1998 Electrical stimulation of the subthalamic nucleus in advanced Parkinson's disease *New Engl. J. Med.* **339** 1105–11
- Löhler P, Albert A, Erbslöh A, Nruthyathi F M and Seidl K 2023 A cell-type selective stimulation and recording system for retinal ganglion cells *IEEE Trans. Biomed. Circuits Syst.* **1–13**
- Lohmann T K, Haiss F, Schaffrath K, Schnitzler A-C, Waschkowski F, Barz C, van Der Meer A-M, Werner C, Johnen S and Laube T 2019 The very large electrode array for retinal stimulation (VLARS)—a concept study *J. Neural Eng.* **16** 066031
- Lorach H *et al* 2015 Photovoltaic restoration of sight with high visual acuity *Nat. Med.* **21** 476–82
- Lorach H *et al* 2023 Walking naturally after spinal cord injury using a brain-spine interface *Nature* **618** 126–33
- Madugula S S *et al* 2022 Focal electrical stimulation of human retinal ganglion cells for vision restoration *J. Neural Eng.* **19** 066040
- Mankowska N D, Marcinkowska A B, Waskow M, Sharma R I, Kot J and Winkowski P J 2021 Critical flicker fusion frequency: a narrative review *Medicina* **57** 1096
- Mueller J K and Grill W M 2013 Model-based analysis of multiple electrode array stimulation for epiretinal visual prostheses *J. Neural Eng.* **10** 036002
- Muqit M M K, Velikay-Parel M, Weber M, Dupeyron G, Audemard D, Corcostegui B, Sahel J and Le Mer Y 2019 Six-month safety and efficacy of the intelligent retinal implant system II device in retinitis pigmentosa *Ophthalmology* **126** 637–9
- Nanduri D, Fine I, Horsager A, Boynton G M, Humayun M S, Greenberg R J and Weiland J D 2012 Frequency and

- amplitude modulation have different effects on the percepts elicited by retinal stimulation *Invest. Ophthalmol. Vis. Sci.* **53** 205–14
- Oesterle J, Behrens C, Schröder C, Hermann T, Euler T, Franke K, Smith R G, Zeck G and Berens P 2020 Bayesian inference for biophysical neuron models enables stimulus optimization for retinal neuroprosthetics *Elife* **9** e54997
- Paknahad J, Loizos K, Humayun M and Lazzi G 2020 Targeted stimulation of retinal ganglion cells in epiretinal prostheses: a multiscale computational study *IEEE Trans. Neural Syst. Rehabil. Eng.* **28** 2548–56
- Plachta D T, Gierthmuehlen M, Cota O, Espinosa N, Boeser F, Herrera T C, Stieglitz T and Zentner J 2014 Blood pressure control with selective vagal nerve stimulation and minimal side effects *J. Neural Eng.* **11** 036011
- Radivojevic M, Jackel D, Altermatt M, Muller J, Viswam V, Hierlemann A and Bakkum D J 2016 Electrical identification and selective microstimulation of neuronal compartments based on features of extracellular action potentials *Sci. Rep.* **6** 31332
- Rattay F 1988 Modeling the excitation of fibers under surface electrodes *IEEE Trans. Biomed. Eng.* **35** 199–202
- Rattay F, Paredes L P and Leao R N 2012 Strength-duration relationship for intra- versus extracellular stimulation with microelectrodes *Neuroscience* **214** 1–13
- Schiefer M A and Grill W M 2006 Sites of neuronal excitation by epiretinal electrical stimulation *IEEE Trans. Neural Syst. Rehabil. Eng.* **14** 5–13
- Schütz H, Steinhoff R, Moll S, Herrmann T, Zeck G and Rothermel A 2020 Pseudo-resistor based attenuator as an efficient electrode driver for sinusoidal stimulation of retinas 2020 *IEEE Int. Symp. on Circuits and Systems (ISCAS)* (IEEE) pp 1–5
- Shah N P and Chichilnisky E J 2020 Computational challenges and opportunities for a bi-directional artificial retina *J. Neural Eng.* **17** 055002
- Spencer T C, Fallon J B, Thien P C and Shivdasani M N 2016 Spatial restriction of neural activation using focused multipolar stimulation with a retinal prosthesis *Invest. Ophthalmol. Vis. Sci.* **57** 3181–91
- Steins H, Mierzejewski M, Brauns L, Stumpf A, Kohler A, Heusel G, Corna A, Herrmann T, Jones P D and Zeck G 2022 A flexible protruding microelectrode array for neural interfacing in bioelectronic medicine *Microsyst. Nanoeng.* **8** 131
- Stupak N, Padilla M, Morse R P and Landsberger D M 2018 Perceptual differences between low-frequency analog and pulsatile stimulation as shown by single- and multidimensional scaling *Trends Hear.* **22** 2331216518807535
- Twyford P and Fried S 2016 The retinal response to sinusoidal electrical stimulation *IEEE Trans. Neural Syst. Rehabil. Eng.* **24** 413–23
- Vagni P, Airaghi Leccardi M J I, Vila C H, Zollinger E G, Sherafatipour G, Wolfensberger T J and Ghezzi D 2022 POLYRETINA restores light responses in vivo in blind Gottingen minipigs *Nat. Commun.* **13** 3678
- Weitz A C, Nanduri D, Behrend M R, Gonzalez-Calle A, Greenberg R J, Humayun M S, Chow R H and Weiland J D 2015 Improving the spatial resolution of epiretinal implants by increasing stimulus pulse duration *Sci. Transl. Med.* **7** 318ra203
- Werginz P, Raghuram V and Fried S I 2020 The relationship between morphological properties and thresholds to extracellular electric stimulation in  $\alpha$  RGCs *J. Neural Eng.* **17** 045015
- Wilson B S and Dorman M F 2008 Cochlear implants: current designs and future possibilities *J. Rehabil. Res. Dev.* **45** 695–730
- Xie T, Vigil J, MacCracken E, Gasparaitis A, Young J, Kang W, Bernard J, Warnke P and Kang U J 2015 Low-frequency stimulation of STN-DBS reduces aspiration and freezing of gait in patients with PD *Neurology* **84** 415–20
- Zeck G, Jetter F, Channappa L, Bertotti G and Thewes R 2017 Electrical imaging: investigating cellular function at high resolution *Adv. Biosyst.* **1** 1700107
- Zeck G, Lambacher A and Fromherz P 2011 Axonal transmission in the retina introduces a small dispersion of relative timing in the ganglion cell population response *PLoS One* **6** e20810
- Zeitler R, Fromherz P and Zeck G 2011 Extracellular voltage noise probes the interface between retina and silicon chip *Appl. Phys. Lett.* **99** 263702
- Zhou M, Young B K, Della Valle E D, Koo B, Kim J and Weiland J D 2023 Full-field, conformal epiretinal electrode array using hydrogel and polymer hybrid technology *Sci. Rep.* **13** 6973